PERGAMON

Journal of Structural Geology 23 (2001) 733–743

JOURNAL OF STRUCTURAL GEOLOGY

www.elsevier.nl/locate/jstrugeo

Analogue models of transpressive systems

A.M. Casas[a,*], D. Gapais[b], T. Nalpas[b], K. Besnard[b], T. Román-Berdiel[a]

[a]*Departamento de Ciencias de la Tierra, Universidad de Zaragoza, 50009 Zaragoza, Spain*
[b]*Géosciences Rennes, Université de Rennes 1, Campus de Beaulieu, Av. du Général Leclerc, 35000 Rennes Cedex, France*

Received 14 February 2000; accepted 23 October 2000

Abstract

This paper presents three series of analogue models of transpressional deformation in a brittle/ductile system: (1) simple transpression, (2) transpression combined with erosion of uplifted areas of the hanging wall above the deformation front, and (3) transpression combined with erosion of the hanging wall and sedimentation at the foot of uplifted zones. In each series of experiments, different convergence angles α, from 0° (pure wrenching) to 90° (pure thrusting) were applied to the models. Results show a sharp contrast between structures formed at $\alpha \leq 15°$ (wrench-dominated transpression) and $\alpha \geq 30°$ (thrust-dominated transpression). For a low convergence/strike-slip ratio ($0° \leq \alpha \leq 15°$), the deformation is localized and structures are typical of a strike-slip regime (R and Y faults). For higher convergence angles ($30° \leq \alpha \leq 90°$), the deformation is similar for all models, with an elongate asymmetric uplift showing fault-propagation-fold geometries and flanked by thrust-wrench faults. Fault dips also show a significant change from more than 70° for $\alpha \leq 15°$ to less than 40° for $\alpha > 30°$. For $\alpha \geq 30°$, the geometry of the main faults at the borders of the uplift zone is modified by P faults. In experiments with erosion and sedimentation, and thrust-dominated transpression, new faults with increasing dips form during progressive deformation, branching on the main fault at the base of the model. © 2001 Elsevier Science Ltd. All rights reserved.

Keywords: Transpression; Analogue modelling; Erosion; Sedimentation

1. Introduction

Transpression results in combinations of wrenching and thrusting structures (e.g. Harland, 1971; Sanderson and Marchini, 1984; Woodcock and Schubert, 1994; Dewey et al., 1998). It can be related to particular boundary conditions at the regional scale, such as an obliquity between the imposed shear motion and pre-existing major faults or oblique convergence at plate boundaries (Tikoff and Teyssier, 1994). It can also occur at the local scale, for example at compressive jogs along a strike-slip fault (Sanderson and Marchini, 1984; Davison, 1994; Keller et al., 1997). Common structures associated with transpression are so-called positive flower structures or palm-tree structures (Wilcox et al., 1973; Sylvester and Smith, 1976; Harding, 1985; Sylvester, 1988). The structures are defined by a series of anastomosing convex-upward faults, with gentle dips at the surface, which steepen progressively at depth, and finally branch on a single subvertical fault zone. At the scale of plate tectonics, transpressive motion caused by oblique convergence can be expressed by a single fault zone or it can be partitioned (Karig et al., 1980; Cobbold et al., 1991; Tikoff and Teyssier, 1994; Jones and Tanner, 1995).

Erosion and sedimentation influence the development of geological structures (e.g. Koons, 1990; Beaumont et al., 1992; Mugnier et al., 1997; Barrier et al., 2001; see also Merritt and Ellis, 1994 and references therein). According to the first authors, asymmetric rainfall across an orogen may result in asymmetry in its tectonic evolution. Barrier et al. (2001) determined the conditions of development of break-back thrust sequences due to sedimentation at the front of thrust systems. The role of erosion and sedimentation in transpressional deformation has been analysed from the geometrical and mechanical points of view by Koons (1994), and field examples are found in several mountain belts, such as the Southern Alps of New Zealand or the Tien–Shan Kazanstua (Norris and Cooper, 1997; Tibaldi, 1998).

Theoretical aspects of transpressive kinematics have been extensively studied (Sanderson and Marchini, 1984; Fossen and Tikoff, 1993, 1998; Fossen et al., 1994; Tikoff and Teyssier, 1994; Krantz, 1995; Dutton, 1997; Jones et al., 1997; Merle and Gapais, 1997; Dewey et al., 1998). Alternatively, only a few studies of transpressional structures based on analogue modelling have been performed. Hoeppener et al. (1969) and Lowell (1972) using clay

* Corresponding author. Fax: +34-976-761088.
E-mail address: acasas@posta.unizar.es (A.M. Casas).

0191-8141/01/$ - see front matter © 2001 Elsevier Science Ltd. All rights reserved.
PII: S0191-8141(00)00153-X

published the first approaches. Lowell (1972) described the deformation of clay cakes over rigid plates, with an angle of 15° between the convergence direction and a basal underlying discontinuity. Wilcox et al. (1973) described structural differences between a pure strike-slip regime, 2° convergent strike-slip faults, and 15° convergent faults. In a pure strike-slip regime, the fault pattern that develops consists of synthetic oblique faults with Riedel attitude (R faults), antithetic faults (R′ faults) at high angles to the bulk shear direction, synthetic P faults, symmetric to R faults, and Y faults, subparallel to the bulk shear direction (Tchalenko, 1970). Structures formed with a convergence angle of 2° were oblique "en-échelon" folds at high angles to the shear direction. Those formed with a convergence angle of 15° were marked by thrusts at both sides of a deformed uplifted area and cut by numerous R faults.

Brittle–ductile analogue systems submitted to transpression were studied by Richard and Cobbold (1990) and Richard et al. (1991), who analysed the deformation above low-angle and high-angle basement faults, and by Richard and Krantz (1991) who studied the effects of reactivation of high-angle basement faults below a sand–silicone model under pure thrusting and pure wrenching conditions. They obtained steeply dipping faults within the sand layer, with partitioning of the deformation between strike-slip faults and thrusts, caused by a two-stage deformation history (first compression, then strike-slip) imposed by the model. More recently, strain patterns related to oblique convergence were studied by Koons and Henderson (1995) using sand box models. Other models have been developed by Keller et al. (1997) to study geometries of structures in fault jogs. Recently, Schreurs and Colletta (1998) performed transpression experiments using brittle models made of sand and glass powder. Finally, Tikoff and Peterson (1998) have studied the effect of transpression on the reorientation of folds.

The aim of the present study is to analyse structures induced by transpression in a sedimentary cover, with an underlying detachment level, using two-layer analogue models made of a basal ductile silicone layer overlain by a sand layer. Analogue experiments such as these are particularly convenient to model structures developed above a shallow crustal décollement level. The effects of three factors are examined: the convergence angle, the erosion of uplifted areas, and the sedimentation at the foot of major uplifted zones.

2. Experimental procedure

Modelling techniques used have been described in detail in several studies made previously at the experimental laboratory of Géosciences Rennes (Rennes University) (e.g. Faugère and Brun, 1984; Davy and Cobbold, 1988; Tron and Brun, 1991). Brittle layers are made of dry Fontainebleau sand, which has a negligible cohesion, a friction angle of about 30°, and a density around 1400 kg m^{-3} (Krantz, 1991). Ductile layers are made of quasi-newtonian silicone putty (GS1R gum of Rhône – Poulenc), with a viscosity of 10^4 Pa.s at 20°C and a density of about 1270 kg m^{-3}.

The apparatus is a 1 m × 0.5 m box with a mobile wall pushed by two screw jacks driven at constant velocity by a stepper motor (Fig. 1a). The dimensions of the box are sufficiently large to ensure that a large part of the model escapes boundary effects. Attached to the mobile wall is a horizontal rigid plastic sheet, 0.25 m wide, which creates a linear velocity discontinuity at the base of the model near its central part. The two other boundaries are free. The basal plate represents a high-strength basement and the velocity discontinuity may represent either a basement fault, as in experiments by Richard et al. (1991), or the tip line of the basal décollement in an imbricate thrust system (blind thrust, Boyer and Elliot, 1982). At the tip line (tip point in cross-section) detachment folds or fault-propagation folds can form in the sedimentary cover overlying the detachment level.

The models consist of a 1-cm-thick silicone layer overlain by a 2-cm-thick sand pack (Fig. 1a). The sand pack is made of thin alternating coloured layers, which allows the identification of faults and folds on cross-sections. The displacement velocity was constant, 5 cm h^{-1}. For the brittle–ductile ratio of the rheological profile used, this rate is sufficiently fast so that deformation was concentrated above the velocity discontinuity and no deformation occurred near the walls of the model.

Experiments were scaled in terms of gravitational forces, rheology, and strain rates (Hubbert, 1937; Ramberg, 1981; Vendeville et al., 1987). The model ratio for length is 10^{-5} (1 cm in the model represents 1 km in nature); for stress, 10^{-5} (models are 10^5 times weaker than nature); for time 10^{-9} (1 h represents 100 000 years). Ductile silicone putty is used to model a ductile weak layer interbedded within the brittle crust. Several previous experiments showed that weak layers, such as shales, clays or salt, within the brittle crust were conveniently modelled using silicone layers (Ballard et al., 1987; Vendeville, 1987; Richard et al., 1989, 1991; Basile, 1990). Dry sand layers represent brittle sediments (Hubbert, 1951; Horsfield, 1977). We used a displacement velocity of 5 cm h^{-1}, which scales to 10^{-9} m s^{-1} (5 cm a^{-1}). For the chosen brittle/ductile ratio (2:1), this displacement rate is convenient to model upper-crustal processes, like thrusting above a décollement level (for details on scaling of sand-silicone models, see Vendeville et al., 1987 and Davy and Cobbold, 1988). The displacement velocity used is convenient for regions undergoing high strain rates, like active ductile thrust zones, such as the Piute Mountains (southeastern California, Karlstrom et al., 1993), or the Alpine fault of New Zealand (Norris and Cooper, 1997).

During experiments, photographs of the surface of models were taken at regular time intervals to study the

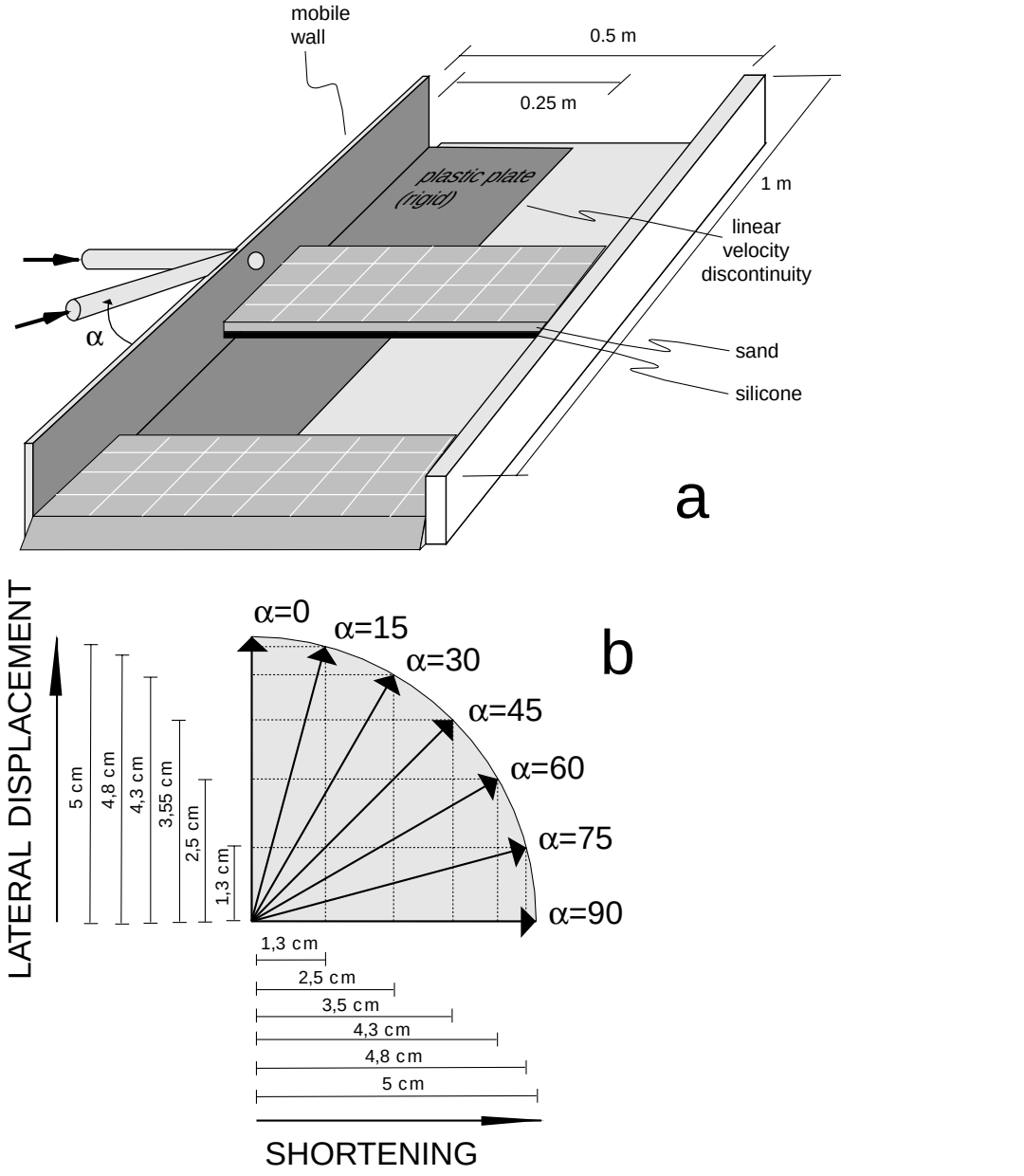

Fig. 1. (a) Experimental apparatus and model setting. (b) Displacement vector (with amounts of strike-slip and convergent displacements) for the different experiments; α is the convergence angle.

progressive evolution of structures (Fig. 2a). At the end of each experiment, the geometry of structures and their changes along strike were observed on serial cross-sections (Fig. 2b). To check the consistency of the results obtained, some of the experiments were repeated. They yielded very similar geometries in plan-view and cross-section.

Three series of experiments, with a systematic variation of the bulk convergence direction, between shortening perpendicular to the velocity discontinuity and pure strike-slip were carried out (Fig. 1b). The variable investigated was the angle α, defined as the angle of obliquity between the displacement direction and the velocity discontinuity (VD) (Withjack and Jamison, 1986; Tron and Brun 1991). For pure strike-slip, $\alpha = 0°$, and for pure convergence, $\alpha = 90°$. The duration of deformation, and therefore the total length of displacement vectors of points located on the mobile plate, was 5 cm in all experiments. The first series of experiments (seven models, from $\alpha = 0°$ to $\alpha = 90°$) was carried out without erosion and sedimentation. In this series, a squared grid of passive coloured markers was drawn on the upper surface of models to study the progressive deformation in plan view (Fig. 2a). In a second series of experiments, uplifted areas above the velocity discontinuity were subjected to erosion during deformation. In a third series of experiments, both erosion of the fault hanging wall and sedimentation at the fault footwall were simulated.

As no structural uplift formed during deformation when $\alpha = 0°$, only six experiments were carried out in the second and third series. In models with erosion and (or) sedimentation, only the final geometry in cross-sections can be observed.

Removal of material (erosion) and addition of material (sedimentation) were made at regular time intervals of 12 min during the experiments, corresponding to 1 cm of total displacement. Local excess topography was removed by sucking up the sand using a small hoover vacuum, leaving a differential topography of at most 2 mm between the highest and the lowest topographic levels. This implies maximum slope angles between 5 and 10°. For $\alpha = 15°$, because of very limited uplift, the differential topography after erosion was 1 mm only. Sedimentation was simulated by sprinkling dry sand onto the model surface, at the foot of the main area of relief formed during deformation.

The erosion applied created not exactly a flat topography, but a low relief area (2 mm in the model, equivalent to 200 m in nature) with gentle slopes. This situation may be equivalent to natural examples found in both marine and continental environments (see for example, Poblet and Hardy, 1995; Zapata and Allmendinger, 1996; Poblet et al., 1997). Sedimentation was applied to the sides of the elevated area, to finally join the flat surface of the non-deformed parts of the model, 5–10 cm away from the central uplift. The slope angle of the sedimentation surface was between 2 and 5°, a common value in many depositional environments, as, for example, areas with alluvial fan sedimentation close to subaerial tectonic uplifts, or carbonate and marl sedimentations on underwater marine slopes (Reading, 1996).

3. Simple transpressive experiments

In all experiments, the deforming area is located above the basal velocity discontinuity. In all models (except for $\alpha = 0°$) the main fault structures were oblique-slip faults, and no slip-partitioned system of parallel strike-slip and thrust faults developed (Fig. 3). Another important feature of the series of experiments is the sharp contrast between experiments with $\alpha \leq 15°$ and $\alpha \geq 30°$ (Figs. 3 and 4).

For $\alpha \leq 15°$, the deformation is basically of the strike-slip type: a shear band containing synthetic Riedel-type faults developed above the velocity discontinuity (Fig. 3). For pure strike-slip, R faults lie at about 15° to the bulk shear direction and are accompanied by Y-type faults subparallel to the bulk shear direction (Fig. 3b). No significant uplift is observed, attesting to bulk plane strain. Similar patterns are classically observed in simple shear experiments (Tchalenko, 1970; Naylor et al., 1986; Basile, 1990; Tron and Brun, 1991). For $\alpha = 15°$, secondary faults formed at angles of about 25° to the bulk shear direction, and Y faults are not observed. The relief developed in the deformation band remained moderate (Fig. 4a).

For $\alpha \geq 30°$, a 5–7-cm-wide uplift formed above the velocity discontinuity. It is generally bounded by two fault zones (Fig. 4a). Passive markers on models show that the strike-slip component on the two main fault zones decreases with increasing α (Fig. 3). The amount of secondary synthetic Riedel-type faults also decreases. In plan view, for $\alpha = 30°$ to $\alpha = 75°$, the main fault zones appear made of segments with R, P and Y orientations with respect to the basal discontinuity (Fig. 3). R-type orientations are

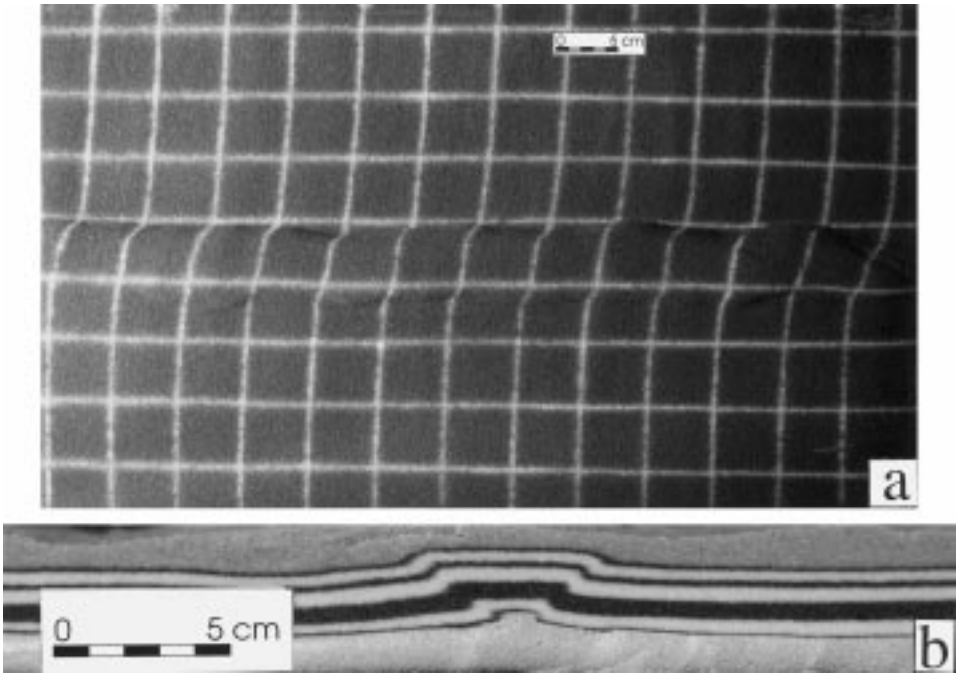

Fig. 2. Photographs showing examples of a deformed model with $\alpha = 30°$, no erosion, and no sedimentation. (a) Surface view of model (shown in the line drawing of Fig. 3d); both Riedel-type orientations and fault segments subparallel to the basal discontinuity are observed. (b) Vertical section across the central part of the model (shown in the line drawing of Fig. 4a); the overall structure is that of a symmetric pop-up.

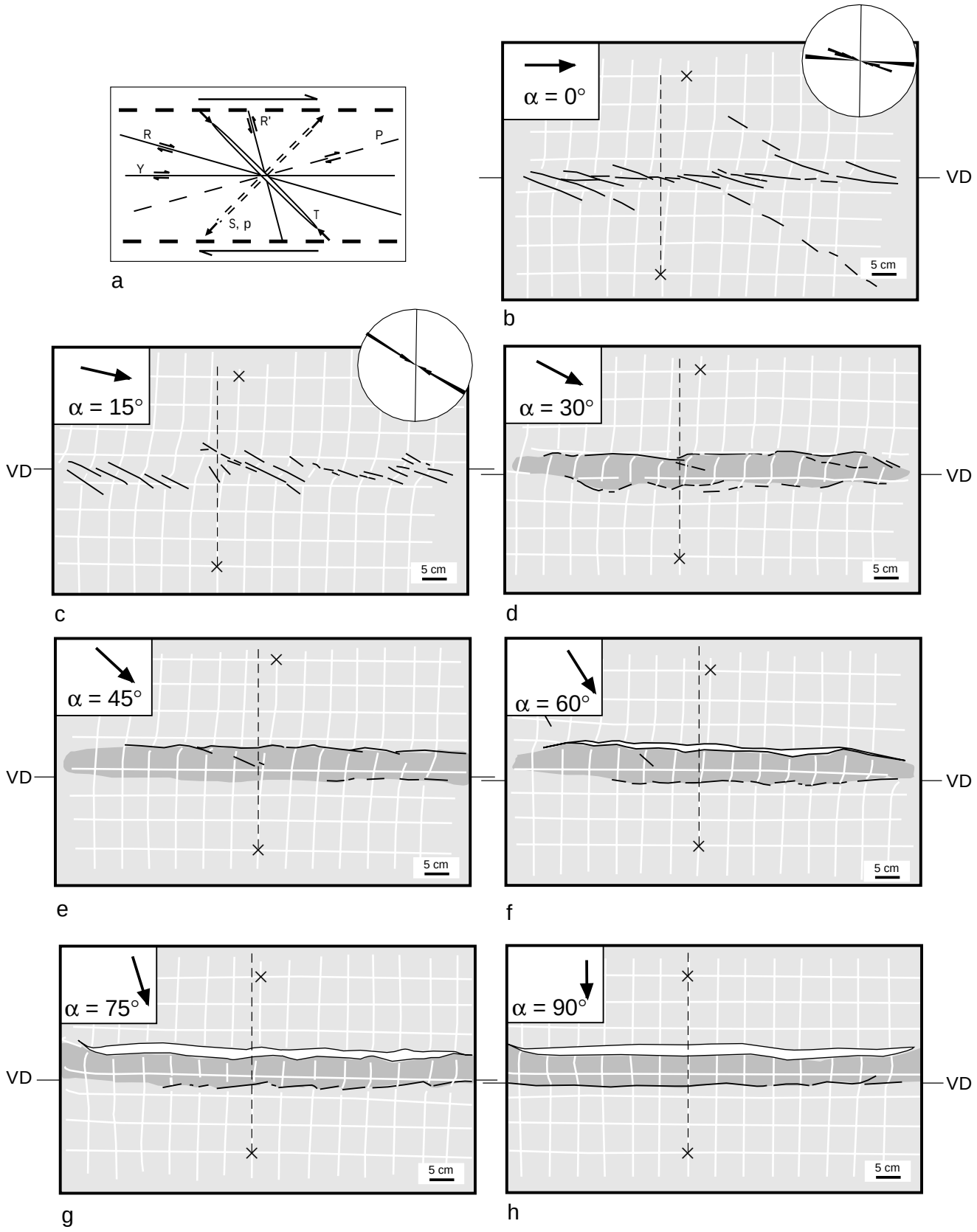

Fig. 3. (a) Examples of different structures that can develop in a strike-slip model shear zone. (b)–(h) Surface views of deformed models without erosion or sedimentation for different convergence angles α. Dark shadowed areas correspond to the uplifted zone (main bulge); white areas to new slopes formed during thrusting, whose dip is determined by the rest angle of sand (30°). In (b) and (c), rose diagrams show preferred orientations of fault traces, weighted by the length of fault segments (radius of circle = 25% of total fault length).

particularly clear in the experiment with $\alpha = 30°$ (Fig. 3d). In the back limb of the uplift, faults with P-type orientation tend to dominate, especially in the experiment with $\alpha = 75°$ (Fig. 3g). These along-strike variations of the orientation of fault traces might reflect local partitioning of strike-slip and thrusting motions, but the resolution of the models is not sufficient to discuss this possibility. In experiments with $\alpha \geq 30°$ most of the strike-slip displacement is accommodated along the frontal oblique-slip fault (closer to the mobile wall). Some, but significantly less, is accommodated at the secondary oblique-slip fault (Fig. 3). The fracture pattern appearing on the central uplift for all these experiments also reveals the strike-slip component, especially along the secondary oblique-slip fault.

For $\alpha = 30°$, the structure in cross-section is almost symmetric, and defines a pop-up bounded by conjugate fault zones (Fig. 4a). In contrast, from $\alpha = 45°$ to $\alpha = 90°$, the geometry of the central uplift in cross-section resembles a fault-propagation fold, nucleated at the velocity discontinuity and verging toward the mobile wall (Fig. 4a). The fault pattern is asymmetric, with the major fault zone located above the mobile plate. The asymmetry is acquired in the initial stages of progressive deformation. On the contrary, for $\alpha = 30°$, the uplift is rather symmetric, although its geometry shows variations along strike (see Fig. 3).

Quantitative relationships between the dip of major faults and the angle of convergence α outline a sharp change between α values of 0 to 15°, where faults are subvertical, and α values equal to or larger than 30°, where fault dips are shallower than 40° (Figs. 4a and 5a). Fault dips were measured on vertical sections perpendicular to the basal velocity discontinuity. For $\alpha \geq 30°$, the overall fault traces at the model surface are parallel or subparallel to the basal discontinuity (Fig. 3). Measured dips are therefore equivalent to real dips. For lower α values, faults are oblique with respect to the basal discontinuity, and real dips would therefore be larger than the measured ones. The change in dip observed between $\alpha = 15°$ and $\alpha = 30°$ thus would be even sharper than shown in Fig. 5a.

For $\alpha \geq 30°$, the dip of the main reverse fault zone at the front limb decreases progressively with increasing α to a minimum dip of 18° for $\alpha = 90°$. This decrease in fault dip with increasing α is accentuated for the upper part of the model, because of a progressive upward change from a footwall ramp to a footwall flat. From $\alpha = 45°$ to $\alpha = 90°$, the decrease in the dip of the main fault can be correlated with an increase in amounts of rotation of the footwall (up to 14° for $\alpha = 90°$). The sum of the two angles is around 30–35° (Fig. 5a), which corresponds to the friction angle of dry sand. Faults at the back limb of folds formed at higher angles (about 40°) in experiments with $\alpha = 30°$ and $\alpha = 60°$. For models with $\alpha = 75°$ and $\alpha = 90°$, their dip is lower, because of back limb rotation and fault-bend folding during thrusting.

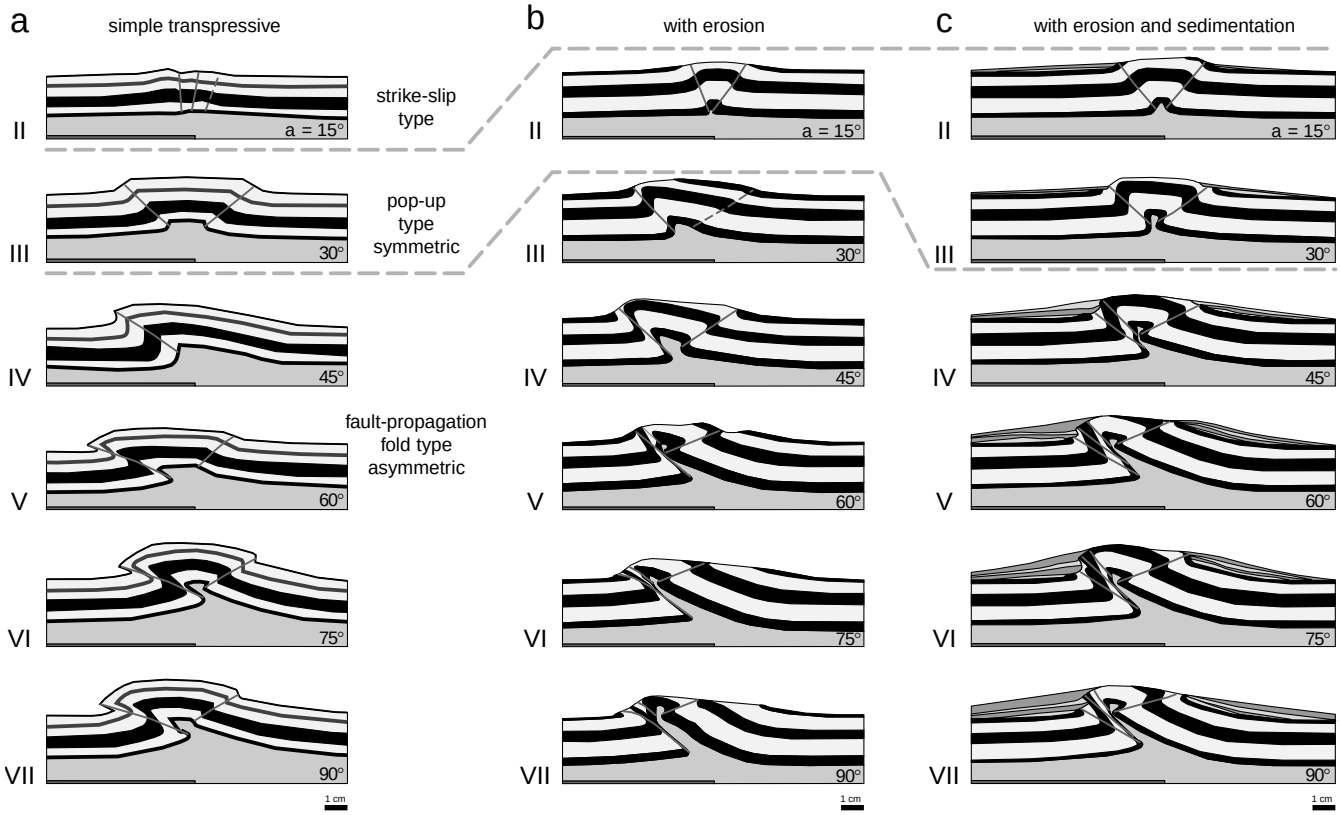

Fig. 4. Cross-sections of deformed models for different convergence angles α. (a) Without erosion or sedimentation, (b) with erosion, and (c) with erosion and sedimentation. Dark grey: silicone layer. Black and light grey: sand layers. The position of the basal mobile plate is shown for each model.

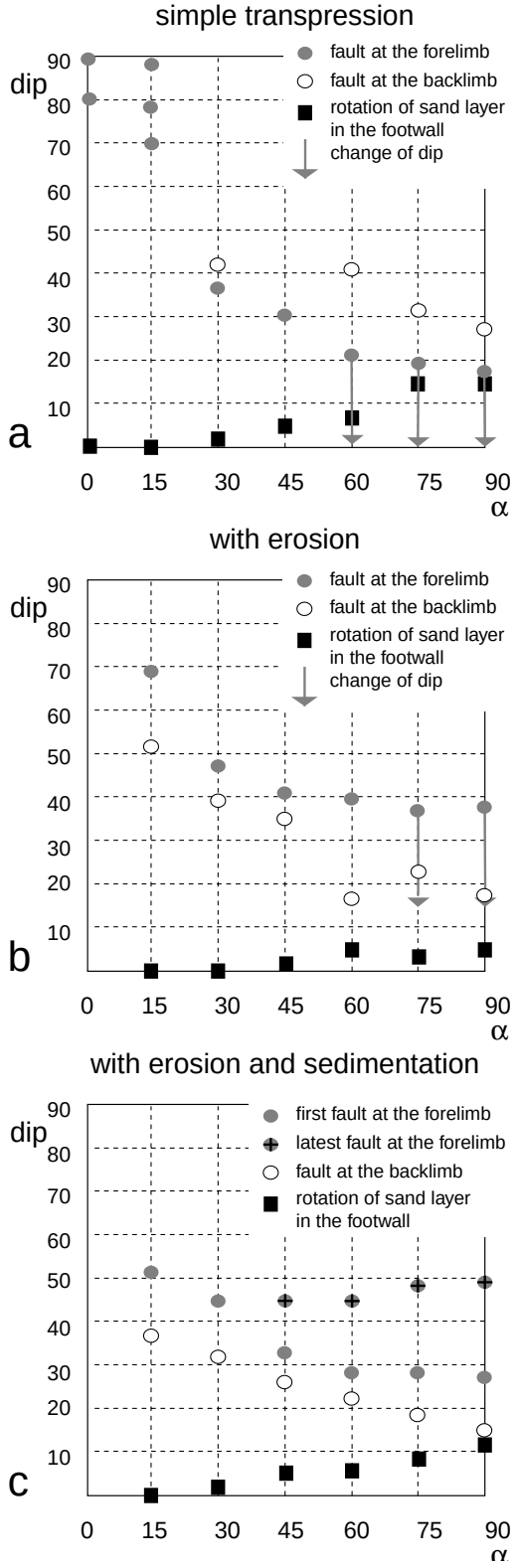

Fig. 5. Diagrams showing relationships between direction, dip, and length of main faults. (a) Without erosion or sedimentation, (b) with erosion, and (c) with erosion and sedimentation.

4. Transpressive experiments with erosion

For $\alpha = 15°$, the overall structure in cross-section is a rather symmetric pop-up (Fig. 4b), comparable with that observed for $\alpha = 30°$ in simple transpressive experiments (Fig. 4a), although it is narrower and the faults are steeper. For $\alpha \geq 30°$ the structure becomes asymmetric, deformation being concentrated in the major fault zone above the mobile plate (Fig. 4b). The relative importance of the forelimb fault zone with respect to that of the back limb increases with increasing α (Fig. 4b). This feature was not clearly observed in experiments without erosion (Fig. 4a). The development of faults at the frontal limb is more important in the series of experiments with erosion, whereas the fault pattern at the back limb is relatively similar to the series without erosion (Fig. 4). Since the markers in the plan view disappear as sand is removed, the deformation pattern associated with the directional component cannot be determined.

Relationships between the dip of faults measured on cross-sections and the angle of convergence α show a change between α values of 15° (dip around 70°) and α values equal to or larger than 30° (dip around 42°) (Fig. 5b). This change in fault dip is less pronounced than in experiments without erosion (Fig. 5a), but it occurs for the same range of α values, between 15 and 30°. For $\alpha \geq 30°$, the dip of the main reverse fault at the front limb decreases slightly from 47 to 38° for $\alpha = 90°$. As in the first series of experiments, the dip of the main fault decreases toward the surface of the model, especially for $\alpha = 75°$ and $\alpha = 90°$. The rotation of the main fault footwall is less pronounced than in simple transpressive experiments, never more than 5°. This may be related to the strong localization of thrust motions within the forelimb fault zone, especially for $\alpha \geq 60°$ (Fig. 4b).

5. Transpressive experiments with erosion and sedimentation

Overall structural patterns are comparable with those observed with erosion alone (Fig. 4b and c). As in the other experiments, a change from pop-up-type structure to asymmetric thrust zone geometry occurs for α values around 30° (Fig. 4c). The main differences with respect to experiments without sedimentation concern the geometry of the major thrust-wrench zone for $\alpha \geq 45°$. In detail, this fault zone is comprised of several individual faults, which developed successively during progressive shortening and sedimentation on the footwall. The earliest fault dips gently, as observed for experiments without sedimentation; but at each subsequent step of erosion/sedimentation applied to the models, a new fault is created, in a break-back sequence and with a steeper dip, and the older faults are covered by sedimentation (Fig. 4c). The overall result is a steepening of the fault zone during progressive deformation. This direct

effect of syntectonic sedimentation at the footwall of thrust zones has been analysed in detail by Barrier et al. (2001).

Consequently, the change observed in the dip of the main fault between $\alpha = 15°$ and $\alpha = 30°$ in the two first series of experiments is not so clear when syntectonic sedimentation occurs (Fig. 5). In the deformed state, the overall dip of the latest faults is around 45–55°, irrespective of the value of α. For $\alpha = 30°$, the dip of the main fault is around 45°. For $\alpha \geq 45°$, the dip of the first fault formed at the front limb decreases progressively as α increases, down to a minimum dip of 27° for $\alpha = 90°$. In contrast, the dip of the latest fault formed tends to increase with increasing α, up to 49° for $\alpha = 90°$. For $\alpha = 60°$, the displacement on the main fault is more important than in simple transpressive experiments. The amount of rotation observed in the footwall of the main fault zone is between that for simple transpressive experiments and that for experiments with erosion. It never exceeds 12° (Fig. 5c).

6. Discussion

6.1. Comparison with previous experiments

The main differences of our models with respect to classical positive flower structures modelled in experiments with clay cakes (Lowell, 1972; Wilcox, 1973) are: (1) the geometry of deformation, and (2) fault patterns. In clay models presented by Lowell (1972) and Wilcox (1973), for low convergence angles ($\alpha = 15°$), two thrusts developed at the borders of the central uplift. In our models, thrust development occurred at higher convergence angles ($\alpha \geq 30°$). This difference can be explained by the existence of a detachment level between the rigid basement and the sand cover. The distribution and attitude of fractures at the model surface for the same convergence angle ($\alpha = 15°$) are also different in the models presented here and in those produced by Lowell (1972) and Wilcox (1973). In our experiments, secondary shear faults (R) form at higher angles (25°) with the shear band than the typical R fractures (formed at 15°) reproduced by these authors.

The structures formed for $\alpha = 30°$, with an oblique fault pattern (high angle R faults) developed on a near symmetric uplift parallel to the velocity discontinuity, are very similar to the results of sandbox experiments shown by Norris and Cooper (1995). Although the experimental conditions are different (indentor instead of plastic plate, no silicone layer, larger displacements and a convergence angle slightly higher, $\alpha = 35°$), the deformation pattern obtained by these authors is strongly consistent with our results. Norris and Cooper (1995) also found, along the Alpine Fault, recent structures that closely resemble the deformation pattern obtained in our $\alpha = 30°$ experiment.

Experiments reproducing the effect of reactivation of a steeply-dipping basement fault in a silicone–sand system under pure dip-slip followed by pure wrench conditions (Richard and Krantz, 1991) resulted in a different deformation pattern. In these experiments faults accommodating the strike-slip and the reverse components were not the same, because of the sequential movement imposed by the main basement fault.

6.2. Wrench-dominated transpression versus thrust-dominated transpression

In the three series of experiments, the general structure is dominated by thrust-type geometries, provided the angle of convergence is 30° or more. This is revealed by: (1) the formation of significant topography for $\alpha \leq 15°$, (2) the formation of structures that resemble flower structures or symmetric pop-up when $\alpha \leq 30°$, and even less when erosion alone is applied to models (Fig. 4b), whereas they show typical thrust geometries when $\alpha \geq 30°$, (3) a change of fault patterns in the map view, from Riedel-type patterns up to $\alpha = 15°$ to faults subperpendicular to the shortening direction for higher convergence angles, and (4) a predominance of moderately dipping faults for $\alpha \geq 30°$. Moreover, patterns where deformation is concentrated within steeply dipping faults are only observed for $\alpha \leq 15°$. Thus, a major switch in deformation patterns occurs for angles of convergence comprised between 15 and 30°. This experimental result is consistent with other arguments suggesting that wrench-dominated transpression changes to thrust-dominated transpression for α values around 20° (Fossen et al., 1994; Tikoff and Teyssier, 1994; Krantz, 1995; Tikoff and Green, 1997; Tikoff and Peterson, 1998). Tikoff and Teyssier (1994) and Teyssier and Tikoff (1998) have emphasized that this change corresponds to a switch in the orientation of the long axis of the infinitesimal strain ellipsoid, from horizontal for $\alpha < 20°$ to vertical for higher convergence angles. It thus seems a simple kinematic effect, a feature consistent with our experimental results. Indeed, if mechanical factors were involved, one could expect substantial influence of erosion and (or) sedimentation on the switch in structural pattern, which is not really observed. A comparable sharp change in structural patterns has been described in analogue modelling of transtension (Withjack and Jamison, 1986; Tron and Brun, 1991).

6.3. Recognition of strike-slip components in nature

For $\alpha > 45°$, the ratio between strike-slip and thrusting components of motion does not have much influence on the geometry of structures, as viewed in cross-section. In map view, the component of strike-slip motion has a moderate influence on the geometry of fault traces, which define an uneven pattern formed by R and P fault segments on both sides of the bulge. This pattern becomes fainter as α increases. Similarly, the geometry in cross-section depends mainly on the angle α, transpressional structures being indistinguishable from those formed during pure thrusting. Moreover, where $\alpha \geq 30°$, experiments indicate that the

dip of major faults is much more influenced by effects of sedimentation and, to a lesser extent of erosion, than by the convergence angle (Fig. 4). This means that in natural transpressional conditions, the component of strike-slip may be difficult to determine, and even to recognize, unless there are reliable markers that can constrain the displacement along strike.

Nevertheless, it must be taken into account that there are other factors, such as the magnitude of the displacement, that could influence the geometry of structures, and limit the application of the experimental results obtained. However, some wrench zone like the Alpine Fault of New Zealand or shear zones cutting across the Sierra Nevada batholith locally show fabrics with steeply plunging stretching lineations, which underline that equivocal relationships can occur between finite strain patterns and bulk horizontal motion (Sibson et al., 1981; Tikoff and Green, 1997).

6.4. Fault attitude in map view

For $\alpha = 15°$, the deformation results in a set of synthetic faults of Riedel-type, but oriented at more than 15° with respect to the bulk shear direction (Fig. 3c). This feature confirms experimental results obtained by Naylor et al. (1986) in strike-slip experiments with pre-stressed sand (compressed with σ_1 perpendicular to the shear band), and those of Krantz (1995) in transpressive experiments. It is also consistent with bulk kinematics: the angle between the short axis of the infinitesimal strain ellipsoid and the overall strike of the shear band imposed by the basal velocity discontinuity is higher for transpression than for simple shear.

The development of faults with P orientation along the back limb of the pop-up is a feature described in other transpressional experiments on clay models (Keller et al., 1997), whereas these fractures rarely appear in simple wrench experiments. Keller et al. (1997) describe P and Y fractures formed along the borders of a pop-up structure at convergence angles higher than 30°. In the models presented here Y fractures do not develop or are substituted by the main oblique-slip fault above the velocity discontinuity. Our results confirm the hypothesis proposed by these authors, that P fractures are mainly associated with transpressional deformation, since they are seldom observed either in experiments of pure strike-slip ($\alpha = 0$) or in wrench-dominated transpression ($\alpha = 15°$) (Fig. 3). Although further comparison, including the progressive development of fractures, is difficult to establish since sand models do not allow the high resolution of clay cakes, another coincidence with the results of Keller et al. (1997) is that in our models, R fractures form generally before P fractures.

6.5. Effects of erosion and sedimentation

In models with erosion, the asymmetry of structures is stronger than in the two other series of experiments. It is well expressed for $\alpha = 30°$ or more, whereas in the first and third series, a minimum convergence angle of 45° seems to be required to generate asymmetric patterns (Fig. 4). In models with erosion and $\alpha \geq 60°$, displacements along faults and deformation are more concentrated along the main front thrust than in the other two series. The deformation zone is narrower and the frontal limb is thinned owing to the displacement of faults cross-cutting this limb. These features can be interpreted as mechanical effects. The removal of the overlying sand originates a decrease of the vertical stress on the fault zone and therefore favours both larger displacements on the fault formed and the formation of new faults cross-cutting the sand cover. This effect of shear softening caused by erosion probably also explains why the displacement along individual faults is higher than in simple transpressive experiments (Figs. 4 and 5), and therefore some of the shortening is accommodated by folding and a larger amount of rotation in the footwall.

In models with erosion and sedimentation, the faults at the front limb are arranged in break-back sequences, a feature that does not appear in the other two series and becomes clearer as the convergence angle α increases. The kinematics of the structure is this series is then determined by sedimentation at the borders of the main bulge. Sand units deposited on the tip of a fault, with an overall onlap geometry, prevent its subsequent movement and a new fault must form, normally where erosion is occurring, that is, in break-back sequence. This can be explained by the sealing of faults by sand during progressive deformation, causing the opposite effect of erosion, explained above. Similar thrust sequences have been described in experiments of *syn*-thrusting sedimentation in sand-silicone models (Barrier et al., 2001). They have also been observed at upper crustal levels in natural transpressional and compressional zones, where break-back sequences are associated with *syn*-tectonic sedimentation covering the older thrust fronts (see, for example, Norris and Cooper, 1997; Pueyo Morer et al., 1999; Barrier et al., 2001).

7. Concluding remarks

From the above series of transpressive experiments on brittle–ductile models, we can draw the following conclusions.

1. The development of fault patterns of strike-slip type requires small convergence angles. Our experimental results are consistent with kinematic analyses that predict a change from wrench-dominated fault systems to thrust-dominated systems for convergence angles of 20° (Tikoff and Teyssier, 1994).
2. The conclusion above emphasizes that strike-slip components in natural transpressive systems might be underestimated or undetected. Furthermore, our experiments show that the development of steeply-dipping faults in thrust dominated situations can be more favoured by

syntectonic sedimentation than by the amount of strike-slip component.

3. The switch from wrench-dominated patterns to thrust-dominated patterns is marked by abrupt changes in: (1) the deformation-induced topography, which, in our experiments, becomes important for $\alpha \geq 15°$, (2) the overall geometry in cross-section, which changes from flower structure or symmetric pop-up to fault-propagation fold geometries, (3) the fault pattern in map view, which changes from Riedel-dominated patterns to fault sets mainly subparallel to the shortening direction, and (4) the overall fault dip which changes from 70–90° to less than 40°.
4. When erosion occurs during deformation, the asymmetry of structures tends to increase and deformation tends to concentrate within the main frontal fault zone. This can be related to shear softening induced by a decrease in lithostatic pressure above the main fault zone.
5. In compression-dominated experiments with erosion and sedimentation, faults develop in break-back sequence with increasing dip, early faults being covered by subsequent deposits on the footwall. It follows that the overall dip of the frontal thrust zone does not vary strongly according to the convergence angle.

Acknowledgements

This work was supported by the project PB97-0997 of the Dirección General de Enseñanza Superior (Ministry of Education, Spain), and by an Integrated Action (Picasso program) of the Ministries of Education of France and Spain. We thank J.J. Kermarrec (Géosciences Rennes) who made and maintained the experimental apparatus and helped during the experiments. We thank Martha Withjack, Richard Norris and James Evans for their constructive and thorough reviews of the manuscript.

References

Ballard, J.F., Brun, J.P., Van den Driessche, J., Allemand, P., 1987. Propagation des chevauchements au-dessus des zones de décollement: modèles experimentaux. Comptes Rendus de l'Académie des Sciences de Paris 305, 1249–1253.

Barrier, L., Nalpas, T., Gapais, D., Proust, J.-N., Casas, A., Bourquin, S., 2001. Relationships between sedimentation and tectonics at the edge of compressive basins. Field study (Iberian Range) and analogue models. Bulletin of the Geological Society of London, in press.

Basile, C., 1990. Analyse structurale et modélisation analogique d'une marge transformante. Exemple de la marge de Côte d'Ivoire-Ghana. Mémoires et Documents du Centre Armoricain d'Etude Structurale des Socles, 39, 220pp.

Beaumont, C., Fullsack, P., Hamilton, J., 1992. Erosional control of active compressional orogens. In: McClay, K.R. (Ed.). Thrust Tectonics. Chapman and Hall, Oxford, pp. 1–18.

Boyer, S.E., Elliott, D., 1982. Thrust systems. American Association of Petroleum Geologists Bulletin 66, 1196–1230.

Cobbold, P.R., Gapais, D., Rossello, E.A., 1991. Partitioning of transpressive motions within a sigmoidal fold belt: the Variscan Sierras Australes, Argentina. Journal of Structural Geology 13, 743–758.

Davison, I., 1994. Linked fault systems: extensional, Strike-slip and contractional. In: Hancock, P.L. (Ed.). Continental Deformation. Pergamon Press, Oxford, pp. 121–142.

Davy, P., Cobbold, P.R., 1988. Indentation Tectonics in nature and experiments. I. Experiments scaled for gravity. Bulletin of the Geological Institut, University of Uppsala 14, 129–141.

Dewey, J.F., Holdsworth, R.E, Strachan, R.A., 135. Transpression and transtension zones. In: Holdsworth, R.E., Strachan, R.A., Dewey, J.F. (Eds.). Continental Transpressional and Transtensional Tectonics. Geological Society Special Publication, London, pp. 1–13.

Dutton, B.J., 1997. Finite strains in transpression zones with no boundary slip. Journal of Structural Geology 19, 1189–1200.

Faugère, E., Brun, J.P., 1984. Modélisation expérimentale de la distension continentale. Comptes Rendus de l'Académie des Sciences de Paris II 299 (7), 265–270.

Fossen, H., Tikoff, B., 1993. The deformation matrix for simultaneous simple shearing, pure shearing, and volume change, and its application to transpression/transtension tectonics. Journal of Structural Geology 15, 413–422.

Fossen, H., Tikoff, B., 1998. Extended models of transpression and transtension, and application to tectonic settings. In: Holdsworth, R.E., Strachan, R.A., Dewey, J.F. (Eds.). Continental Transpressional and Transtensional Tectonics. Geological Society of London Special Publication 135, pp. 15–33.

Fossen, H., Tikoff, B., Teyssier, C., 1994. Strain modelling of transpressional and transtensional deformation. Norsk Geologisk Tidsskrift 74, 134–145.

Harding, T.P., 1985. Seismic characteristics and identification of negative flower structures, positive flower structures and positive structural inversion. American Association of Petroleum Geologists Bulletin 69 (4), 582–600.

Harland, W.B., 1971. Tectonic transpression in Caledonian Spitzbergen. Geological Magazine 108, 27–42.

Hoeppener, R., Kalthoff, E., Schrader, P., 1969. Zur physikalischen Tektonik: Bruchbildung bei verschidenen affinen Defomationen im Experiment. Geologische Rundschau 59, 179–193.

Horsfield, W.T., 1977. An experimental approach to basement-controlled faulting. Geologie en Mijnbouw 56 (4), 363–370.

Hubbert, M.K., 1937. Theory of scale models as applied to the study of geologic structures. Geological Society of America Bulletin 48, 1459–1520.

Hubbert, M.K., 1951. Mechanical basis for certain familiar geologic structures. Geological Society of America Bulletin 62 (4), 355–372.

Jones, R.R., Tanner, P.W., 1995. Strain partitioning in transpression zones. Journal of Structural Geology 17, 793–802.

Jones, R.R., Hodsworth, R.E., Bailey, W., 1997. Lateral extrusion in transpression zones: the importance of boundary conditions. Journal of Structural Geology 19, 1201–1217.

Karig, D., Lawrence, M.B., Moore, G.F., Curray, J.R., 1980. Structural framework of forearc basin, NW Sumatra. Journal of the Geological Society, London 137, 77–91.

Karlstrom, K.E., Miller, C.F., Kingsbury, J.A., Wooden, J.L., 1993. Pluton emplacement along an active ductile thrust zone, Piute Mountains, southeastern California: interaction between deformation and solidification processes. Geological Society of America Bulletin 105, 213–230.

Keller, J.V.A., Hall, S.H., McClay, K.R., 1997. Shear fracture pattern and microstructural evolution in transpressional fault zones from field and laboratory studies. Journal of Structural Geology 19, 1173–1187.

Koons, P.O., 1990. Two-sided orogen: collision and erosion from the sandbox to the Southern Alps, New Zealand. Geology 18, 679–683.

Koons, P.O., 1994. Three-dimensional critical wedges: tectonics and topography in oblique collisional orogens. Journal of Geophysical Research 99 (B6), 12301–12315.

Koons, P.O., Henderson, C.M., 1995. Geodetic analysis of model oblique

collision and comparison to the Southern Alps of New Zealand. New Zealand Journal of Geology and Geophysics 38, 545–552.

Krantz, R.W., 1991. Measurements of friction coefficients and cohesion for faulting and fault reactivation in laboratory models using sand and mixtures. Tectonophysics 188, 203–207.

Krantz, R.W., 1995. The transpressional strain model applied to strike-slip, oblique-convergent and oblique-divergent deformation. Journal of Structural Geology 17, 1125–1137.

Lowell, J.D., 1972. Spitsbergen Tertiary orogenic belt and the Spitsbergen fracture zone. Geological Society of America Bulletin 83, 3091–3102.

Merle, O., Gapais, D., 1997. Strains within thrust-wrench zones. Journal of Structural Geology 7, 1011–1014.

Merritt, D., Ellis, M., 1994. Introduction to special section on tectonics and topography. Journal of Geophysisical Research 99 (B6), 12135–12141.

Mugnier, J.L., Baby, P., Colletta, B., Vinour, P., Balé, P., Leturmy, P., 1997. Thrust geometry controlled by erosion and sedimentation: a view from analogue models. Geology 25, 427–430.

Naylor, M.A., Mandl, G., Sijpesteijn, C.H.K., 1986. Fault geometries in basement-induced wrench faulting under different initial stress states. Journal of Structural Geology 8, 737–752.

Norris, R.J., Cooper, A.F., 1995. Origin of small-scale segmentation and transpressional thrusting along the Alpine fault, New Zealand. Geological Society of America Bulletin 107, 231–240.

Norris, R.J., Cooper, A.F., 1997. Erosional control on the structural evolution of a transpressional thrust complex on the Alpine Fault, New Zealand. Journal of Structural Geology 19, 1323–1342.

Poblet, J., Hardy, S., 1995. Reverse modelling of detachment folds: application to the Pico del Aguila anticline in the south central Pyrenees (Spain). Journal of Structural Geology 17, 1707–1724.

Poblet, J., McClay, K., Storti, F., Muñoz, J.A., 1997. Geometries of syntectonic sediments associated with single-layer detachment folds. Journal of Structural Geology 19, 369–381.

Pueyo Morer, E.L., Millán Garrido, H., Pocovi Juan, A., Parés, J.M., 1999. Cinemática rotacional del cabalgamiento basal surpirenaico en las Sierras Exteriores Aragonesas: Datos magnetotectónicos. Acta Geològica Hispànica 32, 237–256.

Ramberg, H., 1981. Gravity, Deformation, and the Earth's Crust in Theory, Experiments and Geological Applications, 2nd edition. Academic Press, New York.

Reading, H.G., 1996. Sedimentary Environments: Processes, Facies and Stratigraphy, 3rd edition. Blackwell, London.

Richard, P., Cobbold, P., 1990. Experimental insights into partitioning of fault motions in continental convergent wrench zones. Annales Teconicae 4, 35–44.

Richard, P., Krantz, R.W., 1991. Experiments on fault reactivation in strike-slip mode. Tectonophysics 188, 117–131.

Richard, P., Ballard, J.F., Colletta, B., Cobbold, P., 1989. Naissance et evolution de failles audessus d'un décrochement de socle: modélisation analogique et tomographie. Comptes Rendus de l'Académie des Sciences de Paris 309, 2111–2118.

Richard, P., Mocquet, B., Cobbold, P.R., 1991. Experiments on simultaneous faulting and folding above a basement wrench fault. Tectonophysics 188, 133–141.

Sanderson, D.J., Marchini, R.D., 1984. Transpression. Journal of Structural Geology 6, 449–458.

Schreurs, G., Colletta, B., 1998. Analogue modelling of faulting in zones of continental transpression and transtension. In: Holdsworth, R.E., Strachan, R.A., Dewey, J.F. (Eds.). Continental transpressional and transtensional tectonics, vol. 135. Geological Society of London Special Publications, pp. 59–79.

Sibson, R.H., White, S.H., Atkinson, B.K., 1981. In: McClay, K.R., Price, N.J. (Eds.). Structure and distribution of fault rocks in the Alpine fault zone, New Zealand. Thrust and nappe tectonics, vol. 9. Geological Society of London Special Publications, pp. 197–210.

Sylvester, A.G., 1988. Strike-slip faults. Geological Society of America Bulletin 100, 1666–1703.

Sylvester, A.G., Smith, R.R., 1976. Tectonic transpression and basement controlled deformation in the San Andreas fault zone, Salton Trough, California. American Association of Petroleum Geologists Bulletin 60 (12), 2081–2102.

Tchalenko, J.S., 1970. Similarities between shear zones of different magnitudes. Bulletin of the Geological Society of America 81, 1625–1640.

Teyssier, C., Tikoff, B., 1998. Strike-slip partitioned transpression of the San Andreas fault system: a lithospheric-scale approach. In: Holdsworth, R.E., Strachan, R.A., Dewey, J.F. (Eds.). Continental Transpressional and Transtensional Tectonics, vol. 135. Geological Society of London Special Publication, pp. 143–158.

Tibaldi, A., 1998. Effects of topography on surface fault geometry and kinematics: examples from the Alps, Italy and Tien Shan, Kazakstan. Geomorphology 24, 225–243.

Tikoff, B., Green, D., 1997. Stretching lineations in transpressional shear zones: an example from the Sierra Nevada Batholith, California. Journal of Structural Geology 19, 29–39.

Tikoff, B., Peterson, K., 1998. Physical experiments of transpressional folding. Journal of Structural Geology 20, 661–672.

Tikoff, B., Teyssier, C., 1994. Strain modelling of displacement-field partitioning in transpressional orogens. Journal of Structural Geology 16, 1575–1588.

Tron, V., Brun, P., 1991. Experiments on oblique rifting in brittle-ductile systems. Tectonophysics 188, 71–84.

Vendeville, B., 1987. Champs de failles et tectonique en extension: Modélisation expérimentale. Mémoires et Documents du Centre Armoricain d'Etude Structurale des Socles. Thèse de Doctorat de l'Université de Rennes I. 15, pp. 5–17.

Vendeville, B., Cobbold, P.R., Davy, P., Brun, J.P., Choukroune, P., 1987. In: Coward, M.P., Dewey, J.F., Hancock, P.L. (Eds.). Physical models of extensional tectonics at various scales. Continental Extensional Tectonics, vol. 28. Geological Society of London Special Publication, pp. 95–107.

Wilcox, R.E., Harding, T.P., Seely, D.R., 1973. Basic wrench tectonics. Association of Petroleum Geologists Bulletin 57 (1), 74–96.

Withjack, M.O., Jamison, W.R., 1986. Deformation produced by oblique rifting. Tectonophysics 126, 99–124.

Woodcock, N.H., Schubert, C., 1994. Continental strike-slip tectonics. In: Hancock, P.L. (Ed.). Continental Deformation. Pergamon Press, pp. 251–263.

Zapata, T.R., Allmendinger, R.W., 1996. Growth stratal records of instantaneous and progressive limb rotation in the Precordillera thrust belt and Bermejo basin, Argentina. Tectonics 15, 1065–1083.